Research Article

Asmat Ullah Yahya, Imran Siddique, Nadeem Salamat, Hijaz Ahmad*, Muhammad Rafiq, Sameh Askar, and Sohaib Abdal

Numerical study of hybridized Williamson nanofluid flow with TC4 and Nichrome over an extending surface

https://doi.org/10.1515/phys-2022-0246
received March 09, 2023; accepted April 28, 2023

Abstract: Enhancement in thermal distribution of Williamson hybrid nanofluid flow is articulated in this research. Nichrome and TC4 nanoparticles are homogenously diffused in the water, which is the base fluid. An elongating surface holds the flow and thermal transition phenomenon in the existence of uniform sources of magnetic field and heat radiation. The boundary of wall obeys a suction and slip condition. The formulation for physical conservation laws is made as a system of partial differential equations. For the solution purpose, their boundary-value problem is transmuted into the ordinary differential form. Then, Matlab code involving Runge–Kutta procedure is run to compute the variation in velocity as well as temperature profiles under impacts of the controlling factors. The comparative computations are made for two cases: nanofluids (TC4 + water) and hybrid nanofluids (TC4, Nichrome + water). The heat for that hybrid nanofluid case is larger than that for the nanofluids. The velocity curve is decreased against increasing magnetic field strength and Williamson parameter. Enhancement in thermal distribution is observed with increasing concentration ϕ_2 of Nichrome.

Keywords: Williamson fluid, hybrid nanofluid, magnetohydrodynamic, Runge–Kutta method

1 Introduction

Nanosized particles are utilized to enhance heat energy conservation, increase the effectiveness of medicines, and improve equipment in medical and engineering fields. Also, when nanosized metallic particles are used in fluid, it change its characteristics that are beneficial in fluid mechanics. Normally, these nanosized particles are constructed by carbides, oxides, metals, *etc*. By using the nanoparticles, Hazarika *et al*. [1] discussed the thermophoresis process in the nanofluid. Berrehal *et al*. [2] predicted the shape impacts of nanoparticles on stretching sheet. On the unsteady fluid, the effects of nanoparticle were investigated by Tlili *et al*. [3]. Zahmatkesh *et al*. [4] analyzed the thermal system by using the nanoparticle impacts. The study of radiative nanofluid stream in the presence of nanoparticles was predicted by Acharya *et al*. [5]. The investigation of non-isothermal system containing nanoparticles was described by Abbas *et al*. [6]. He *et al*. [7] investigated the theory of harvesting of energy with carbon nanotube-embedded boundary-layer. Gorji *et al*. [8] showed how they used X-ray diffraction technique to examine the surface of an IC chip without causing any damage.

The fluids that are independent of stress or having constant viscosity are classified as non-Newtonian fluids. Also, Newton's laws of viscosity are not applicable for non-Newtonian fluids. At present these fluids are widely

* **Corresponding author: Hijaz Ahmad,** Section of Mathematics, International Telematic University Uninettuno, Corso Vittorio Emanuele II, 39,00186 Roma, Italy; Operational Research Center in Healthcare, Near East University, Near East Boulevard, PC: 99138 Nicosia/Mersin 10, Turkey, e-mail: ahmad.hijaz@uninettuno.it
Asmat Ullah Yahya, Nadeem Salamat: Department of Mathematics, Khwaja Fareed University of Engineering and Information Technology, Rahim Yar Khan, Pakistan
Imran Siddique: Department of Mathematics, University of Management and Technology, Lahore, Pakistan
Muhammad Rafiq: Department of Mathematics, COMSATS University Islamabad, Wah Campus, 47040, Wah Cantt, Pakistan
Sameh Askar: Department of Statistics and Operations Research, College of Science, King Saud University, P.O. Box 2455, Riyadh 11451, Saudi Arabia
Sohaib Abdal: Department of Mathematics, Khwaja Fareed University of Engineering and Information Technology, Rahim Yar Khan, Pakistan; School of Mathematics, Northwest University, No. 229 North Taibai Avenue, Xi'an 7100069, China

used in engineering, medical fields, and daily life. Non-Newtonian fluids are most commonly encountered as melted butter, ketchup, shampoo, corn starch, apple juice, and starch suspensions. Williamson fluid is an important non-Newtonian fluid, which was introduced by Williamson in 1929 [9]. This fluid is used in different areas such as fluid film condensation process, emulsion coating on photographic films, and behavior of pseudo-plastic fluid that is extensively used in industrial applications. Yahya *et al.* [10] scrutinized the enhancement of thermal application of Williamson hybrid nanofluids using different nanoparticles. The study of Williamson nanofluid with inclined magnetic field was examined by Abdelmalek *et al.* [11]. Wang *et al.* [12] deliberated the flow of Williamson nanofluid through elastic surface with non-uniform thickness. The impacts on pour stretching sheet with the stream of Williamson nanofluid were depicted by Li *et al.* [13]. Zhou *et al.* [14] analyzed the effects of non-linear Williamson nanofluid on gyrotactic microorganisms.

In recent, decades, many researchers are interested to arrange the hybrid nanofluids. Different investigations have revealed the limitations, applications of single-type nanoparticles, and the attributes of their colloidal mixtures. Al_2O_3-Cu, $Al-Zn$, $TiO_2 + CuO$, *etc.* are the examples of hybrid nanofluids with some base fluids. Zubair *et al.* [15] scrutinized the heat conductivity of the Williamson hybrid nanofluid with radiation effects. The study of thermal and heat transformation in Williamson hybrid nanofluid with chemical reaction was depicted by Nazir *et al.* [16]. Eshgarf *et al.* [17] analyzed the features, formation, and stability analysis of hybrid nanofluids to optimization of energy usage. By using the hybrid nanofluids, Sathyamurthy *et al.* [18] investigated the phenomenon of cooling in photovoltaic penal. The analysis of thermodynamic process in different cycle driven by using hybrid nanofluids in solar collector tubes was carried out by Abid *et al.* [19].

The study of behavior and characteristics of magnetic produced by electrically conducting liquids is known as magnetohydrodynamics (MHD). Alfven [20] was the first who investigated this concept in 1942 and received Noble Prize in 1970. Later on, many researchers put their contribution and use it in many fields of engineering and medical science, such as cooling in refrigerators and electronic devices, medicines, and automobiles. Alblawi *et al.* [21] analyzed the implications of MHD in carbon nanotubes using casson nanofluid. In a cylindrical geometry, MHD effects on carreau nanofluid along different heat source were deliberated by Sabu *et al.* [22]. Rasheed *et al.* [23] studied the analytical study of nanofluid flow over convective boundaries with MHD and chemical impacts. The numerical investigation of nanofluid flow on stretched sheet using MHD to be effective was carried out by Makkar *et al.* [24]. Jimoh *et al.* [25] described the reacting effects of MHD at different thermal conductivity of nanofluid flow with radiation impacts. The study of MHD hybrid nanofluid motion over straining cylinder with non-uniform heat flux was depicted by Ali *et al.* [26].

This work is perceived to examine the enhancement in heat transfer Nichrome and TC4 that are emulgated homogenously in a bulk volume of water. This hybrid nanofluid and heat transition flow across a elongating surface is formulated on the basis of the Williamson fluid model and the Tiweri-Das model. It is presumed that thermal distribution is enhanced and that the application of the results can be helpful in heat exchangers and electronics. This study can further be discussed for a variety of nanofluids to analyze the impacts of thermal properties of materials that are useful for heat transportation phenomena.

2 Mathematical formulation

Williamson nanofluid is presumed to flow in two-dimensions across an elongated surface (Figure 1). The liquid is regarded incompressible, and the stream is convinced to be linear as a result of the dominance of viscous forces inside the boundary-layer flow. The fluid attributes are recognized not to modify with time once the sheet is prolonged in the +ve x-direction with a non-uniform speed.

$$U_w(x, t) = cx,$$

where c signifies the initial straining rate The temperature of an insulated wall is $T_w(x, t) = T_\infty + (cx)$, and this

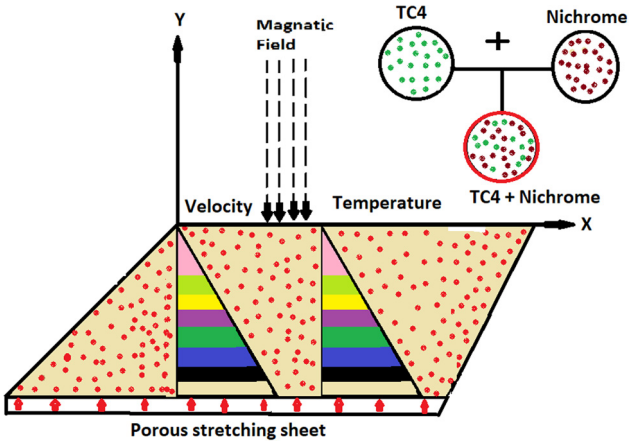

Figure 1: Flowchart.

is supposed to be specified at $x = 0$; for simplicity, here T_w and T_∞ depict the heat of the exterior and surroundings, respectively. A slipping exterior is presumed, and a temperature distribution is adapted to the sheet. In the ordinary direction of flow, a consistent magnetic field of strength $B(t) = B_0$ is initiated.

2.1 Suppositions and conditions of the model

The preceding presumptions and situations are implemented to the problem formulation:

- two-dimensional laminar stable flow,
- varying heat capacity,
- permeable elongating sheet,
- non-Newtonian Williamson nanoparticles,
- MHD,
- boundary-layer approximation,
- heat radiation,
- nanoparticles' shape factor,
- Tiwari and Das model,
- convective and slip boundary situations.

The computational representation of the Williamson liquid stress tensor is presented by:

$$S^* = -pI + \tau_{ij}, \tag{1}$$

where

$$\tau_{ij} = \left[\mu_\infty + \frac{(\mu_0 - \mu_\infty)}{(1 - \phi\tilde{\gamma})}\right]A_1. \tag{2}$$

The governing equations of stream for a viscous Williamson nanofluid were developed and modified using standard boundary-layer estimations, heat radiation, and heat-reliant thermal conductivity.

$$\frac{\partial v_1}{\partial x} + \frac{\partial v_2}{\partial y} = 0, \tag{3}$$

$$v_1\frac{\partial v_1}{\partial x} + v_2\frac{\partial v_1}{\partial y} = \frac{\mu_{hnf}}{\rho_{hnf}}\frac{\partial^2 v_1}{\partial y^2} + \sqrt{2}\Gamma\frac{\mu_{hnf}}{\rho_{hnf}}\frac{\partial v_1}{\partial y}\frac{\partial^2 v_1}{\partial y^2} - \frac{\sigma_{hnf}B_t^2 v_1}{\rho_{hnf}}, \tag{4}$$

$$v_1\frac{\partial T}{\partial x} + v_2\frac{\partial T}{\partial y} = \frac{1}{(\rho C_p)_{hnf}}\left(\frac{\partial}{\partial y}k^*_{hnf}(T)\frac{\partial T}{\partial y}\right) - \frac{1}{(\rho C_p)_{hnf}}\frac{\partial q_r}{\partial y}. \tag{5}$$

With supportive boundary condition,

$$\left.\begin{aligned} &v_1(x,0) = U_w = W^*\mu_{hnf}\frac{\partial v_1}{\partial y}, v_2(x,0) = V^w,\\ &-k_{hnf}\frac{\partial T}{\partial y} = h_f(T_w - T), \quad \text{as } y = 0,\\ &v_1 \to 0, \quad T \to T_\infty, \quad \text{as } y \to \infty. \end{aligned}\right\} \tag{6}$$

Magnetic force term

$$F = qE + qv * B,$$

$$\left.\begin{aligned} &\eta = \sqrt{\frac{c}{\nu_f}}y, \quad u = cxf'(\eta), \quad v = -\sqrt{c\nu_f}\,f(\eta),\\ &\theta(\eta) = \frac{T - T_\infty}{T_w - T_\infty},\\ &k^*_{hnf}(T) = \left(1 + \varepsilon\frac{T - T_\infty}{T_w - T_\infty}\right), \quad \frac{\partial q_r}{\partial y} = -\frac{16T_\infty^3\sigma^*}{3k'k}\frac{\partial^2 T}{\partial y^2}. \end{aligned}\right\} \tag{7}$$

From the aforementioned literature review, the basic thermo-physical characteristics of nanofluids are given in Table 1. The thermo-physical characteristics of water taken as base fluid are given in Table 2. Transformed ordinary differential equations are as follows:

$$f''' - A_1A_2(f'^2 - ff'') + \lambda(f''f''') - A_1A_3Mf' = 0, \tag{8}$$

$$\theta''(1 + \varepsilon\theta + \frac{1}{A_5}\mathrm{PrRd}) + \varepsilon\theta'^2 + \mathrm{Pr}\frac{A_4}{A_5}(f\theta' - f'\theta) = 0, \tag{9}$$

$$\left.\begin{aligned} &f(\eta) = S, \quad f'(\eta) = 1 + \frac{\beta}{A_1}f''(\eta),\\ &\frac{k_{hnf}}{k_f}\theta'(\eta) = B_i(1 - \theta(\eta)), \quad \text{at } \eta = 0,\\ &f'(\eta) \to 0, \quad \theta(\eta) \to 0, \quad \text{as } \eta \to \infty, \end{aligned}\right\} \tag{10}$$

where $M = \frac{\sigma_{hnf}B_t^2}{c\rho_{hnf}}$, $\beta = W^*\sqrt{\frac{c}{\nu_f}}\mu_{hnf}$, $\mathrm{Bi} = \frac{h_f}{k_{hnf}}\sqrt{\frac{\nu_f}{c}}$, $\lambda = \Gamma x\sqrt{\frac{2c^3}{\nu_f}}$, $\mathrm{Pr} = \frac{\nu_f(\rho C_p)_f}{\kappa_f}$, $\mathrm{Rd} = \frac{16T_\infty^3\sigma^*}{3k'k\nu_f(\rho C_p)_f}$, $\mathrm{We} = -V^w\sqrt{\frac{1}{c\nu_f}}$.

Also,

$$A_1 = (1 - \Phi_1)^{2.5}(1 - \Phi_2)^{2.5}\left[(1 - \Phi_2)\left\{(1 - \Phi_1) + \Phi_1\frac{\rho_{s1}}{\rho_f}\right\} + \Phi_2\frac{\rho_{s2}}{\rho_f}\right],$$

$$A_2 = \left[(1 - \Phi_2)\left\{(1 - \Phi_1) + \Phi_1\frac{\rho_{s1}}{\rho_f}\right\} + \Phi_2\frac{\rho_{s2}}{\rho_f}\right],$$

$$A_3 = \left[(1 - \Phi_2)\left\{(1 - \Phi_1) + \Phi_1\frac{(\rho C_p)_{s1}}{(\rho C_p)_f}\right\} + \Phi_2\frac{(\rho C_p)_{s2}}{(\rho C_p)_f}\right],$$

$$A_4 = [(1 - \Phi_1)^{2.5}(1 - \Phi_2)^{2.5}],$$

$$\frac{k_{hnf}}{k_f} = \left[\frac{\kappa_{s2} + (s_f - 1)\kappa_{bf} - (s_f - 1)\Phi_2(\kappa_{bf} - \kappa_{s2})}{\kappa_{s2} + (s_f - 1)\kappa_{bf} + \Phi_2(\kappa_{bf} - \kappa_{s2})}\cdot \frac{\kappa_{s1} + (s_f - 1)\kappa_f - (s_f - 1)\Phi_1(\kappa_f - \kappa_{s1})}{\kappa_{s1} + (s_f - 1)\kappa_f + \Phi_1(\kappa_f - \kappa_{s1})}\right].$$

Table 1: Thermo-physical properties

Physical properties	TC_4	Nichrome	Water
ρ (kg · m^{-3})	4,420	8,314	997.1
C_p (J (kg · ° k))	610	460	4,179
κ (W(m · ° k))	5.8	13	0.613

Physical quantities are

$$C_f = \frac{\tau_w}{\rho_f U_w^2}, \quad \mathrm{Nu} = \frac{x q_w}{k_f(T_w - T_\infty)},$$
$$\tau_w = \mu_{hnf}(1+\Gamma)\left(\frac{\partial u}{\partial y}\right), \; q_w = k_{hnf}\frac{\partial T}{\partial y}, \text{ at } y = 0. \tag{11}$$

Using similarity transformation, we obtain

$$\begin{cases} Cf_x \mathrm{Re}_x^{1/2} = \dfrac{\left(1+\frac{\lambda}{2}\right)f''(0)}{A_4} f''(0), \\ \mathrm{Nu}_x \mathrm{Re}_x^{-1/2} = -\dfrac{[k_{hnf}(1+\mathrm{Rd})\theta'(0)]}{k_f}. \end{cases} \tag{12}$$

3 Numerical scheme

The two-point boundary-value problem, governing the heat and mass transfer problem is highly non-linear. These equations are difficult to yield analytical solution. Numerical and semi-analytical methods [27–37] are suggested for such complex problems. However, semi-analytical methods such as the homotopy perturbation method are used for this purpose [38–41]. Numerical procedure is mostly used for solution of such problems because of easily available computer and variant numerical techniques. Runge–Kutta method is a very effective method [42,43]. The non-linear non-dimensional revised problem and the boundary instances (8) were rectified using the MATLAB built-in code RK-4 strategy and a non-linear shooting methodology. The shooting tactic incorporates the first-order ordinary differential equations (ODEs) and starting instances employing the RK-4 procedure, and deficiency constraints are modified using the shooting technique until the scheme validates the required accuracy. The presence of exponential convergence is affirmed for $\eta_{\max} = 8$. All numerical values acquired in this situation are restricted to a 10^{-5} range. The framework of higher-order differential equations (DEs) is transformed into a structure of first-order basic differential equations using the factors described below.

$$\begin{aligned} s_1' &= s_2, \\ s_2' &= s_3, \\ s_3' &= A_1A_2(s_2 - s_1s_3) - \lambda(s_3s_3') + A_1A_3Ms_2, \\ s_4' &= s_5, \\ s_5'\left(1 + \varepsilon s_4 + \frac{1}{A_5}\mathrm{PrRd}\right) &= -\varepsilon s_5^2 - \mathrm{Pr}\frac{A_4}{A_5}(s_1s_5 - s_2s_4). \end{aligned}$$

In addition to the boundary situations:

$$s_1 = S, \quad s_2 = 1 + \frac{\beta}{A_1}s_3, \frac{k_{hnf}}{k_f}s_5 = B_i(1 - s_4), \quad \text{at } \eta = 0,$$
$$s_2 \to 0, \quad s_4 \to 0 \quad \text{as } \eta \to \infty.$$

4 Results and discussion

The preceding description is used to attain numerical findings from the solutions of Eqs (8)–(10). The influence of the physical factors on the velocity and temperature is noted. The numerical computations are carried out for TC4 and TC4 + Nichrome water-based nanofluids.

Table 2: Thermal characteristics

Properties	Nanofluid	Hybrid nanofluid
μ (viscosity)	$\mu_{nf} = \frac{\mu_f}{(1-\Phi)^{2.5}}$	$\mu_{hnf} = \left[\frac{\mu_f}{(1-\Phi_1)^{2.5}(1-\Phi_2)^{2.5}}\right]$
ρ (density)	$\rho_{nf} = \rho_f(1-\Phi) + \Phi\frac{\rho_s}{\rho_f}$	$\rho_{hnf} = \left[\rho_f(1-\Phi_2)\left((1-\Phi_1) + \Phi_1\frac{\rho_{s1}}{\rho_f}\right) + \Phi_2\rho_{s2}\right]$
ρC_p (heat capacity)	$(\rho C_p)nf = (\rho C_p)_f(1-\Phi) + \Phi\frac{(\rho C_p)_s}{(\rho C_p)_f}$	$(\rho C_p)_{hnf} = \left[(\rho C_p)_f(1-\Phi_2)\left((1-\Phi_1) + \Phi_1\frac{(\rho C_p)_{s1}}{(\rho C_p)_f}\right) + \Phi_2(\rho C_p)_{s2}\right]$
κ (thermal conductivity)	$\frac{\kappa_{nf}}{\kappa_f} = \frac{\kappa_s + (s_f-1)\kappa_f - (s_f-1)\Phi(\kappa_f - \kappa_s)}{\kappa_s + (s_f-1)\kappa_f + \Phi(\kappa_f - \kappa_s)}$	$\frac{\kappa_{hnf}}{\kappa_{bf}} = \left[\frac{\kappa_{s2} + (s_f-1)\kappa_{bf} - (s_f-1)\Phi_2(\kappa_{bf} - \kappa_{s2})}{\kappa_{s2} + (s_f-1)\kappa_{bf} + \Phi(\kappa_{bf} - \kappa_{s2})}\right]$ where $\frac{\kappa_{bf}}{\kappa_f} = \left[\frac{\kappa_{s1} + (s_f-1)\kappa_f - (s_f-1)\Phi_1(\kappa_f - \kappa_{s1})}{\kappa_{s1} + (s_f-1)\kappa_f + \Phi(\kappa_f - \kappa_{s1})}\right]$
σ (electrical conductivity)	$\frac{\sigma_{nf}}{\sigma_f} = 1 + \frac{3(\sigma-1)\Phi}{(\sigma+2) - (\sigma-1)\Phi}$	$\frac{\sigma_{hnf}}{\sigma_{bf}} = \left[1 + \frac{3\Phi(\sigma_1\Phi_1 + \sigma_2\Phi_2 - \sigma_{bf}(\Phi_1+\Phi_2))}{(\sigma_1\Phi_1 + \sigma_2\Phi_2 + 2\Phi\sigma_{bf}) - \Phi\sigma_{bf}((\sigma_1\Phi_1 + \sigma_2\Phi_2) - \sigma_{bf}(\Phi_1+\Phi_2))}\right]$

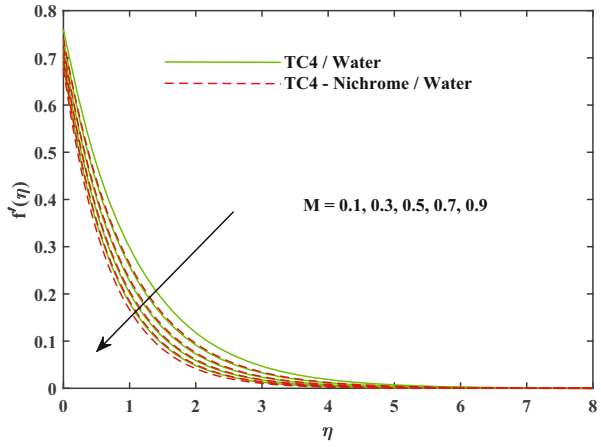

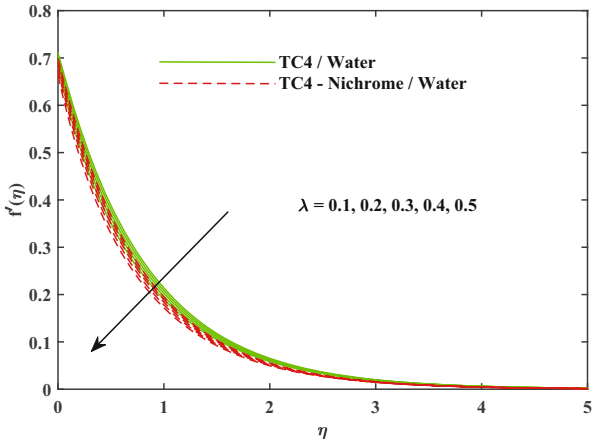

Figure 2: Velocity $f'(\eta)$ fluctuation with M and λ.

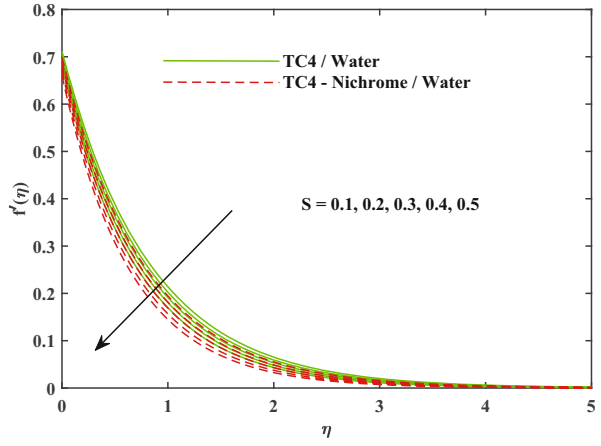

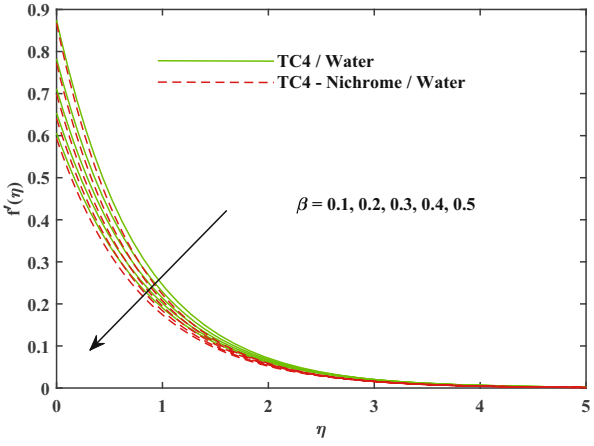

Figure 3: Velocity $f'(\eta)$ fluctuation with S and β.

The graphical attitude of TC4-water nanofluid is depicted in green in the color graphs, whereas the tendency of TC4 + Nichrome–water is exhibited in red.

Figure 2 depicts the implications of the magnetic factor M and Williamson factor λ on the velocity distribution $f'(\eta)$. With a large magnetic factor M, the

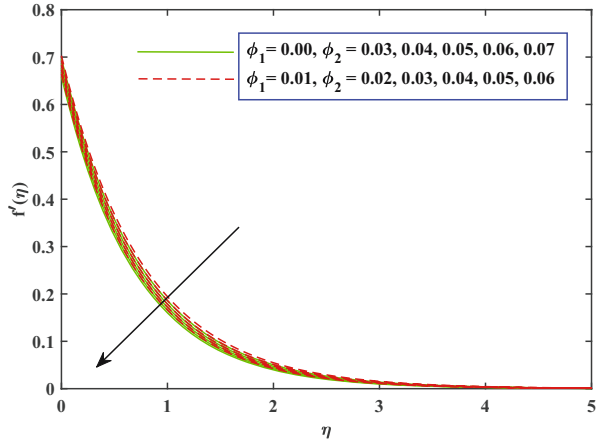

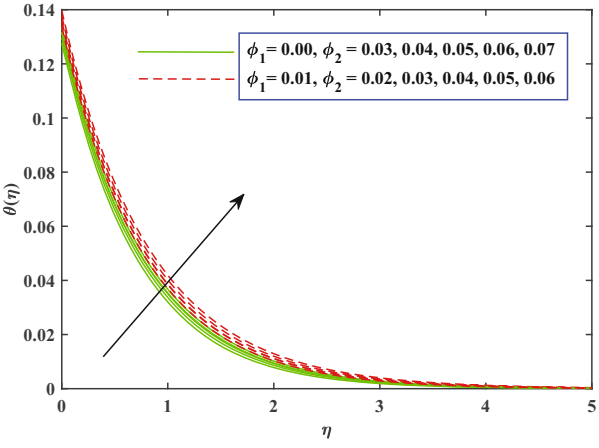

Figure 4: Impact of ϕ_2 on velocity $f'(\eta)$ and temperature $\theta(\eta)$.

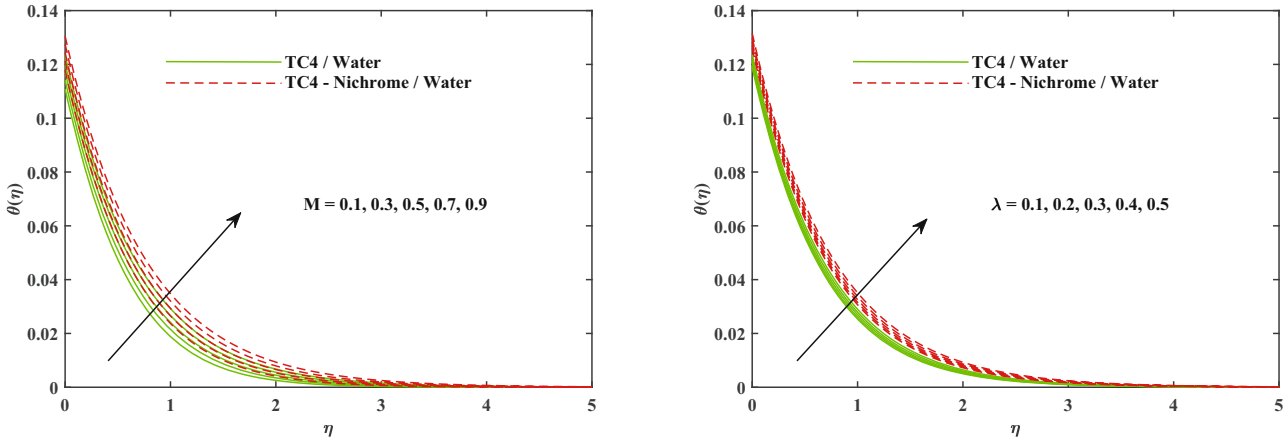

Figure 5: Temperature $\theta(\eta)$ fluctuation with M and λ.

lowering trend of the fluid velocity is seen, leading to a reduction in the depth of the momentum boundary-layer. Actually, Lorentz force emerges when a typically imposed magnetic field reacts with an electric field to retard the boundary-layer thickness. When the intensity of the imposed magnetic force increases, so does the Lorentz force, which works in the reverse way of fluid movement, and thus, the induced fluid friction diminishes the depth of the velocity boundary-layer. The reduction in flow velocity is accompanied by a rise in, as a consequence wherein the momentum

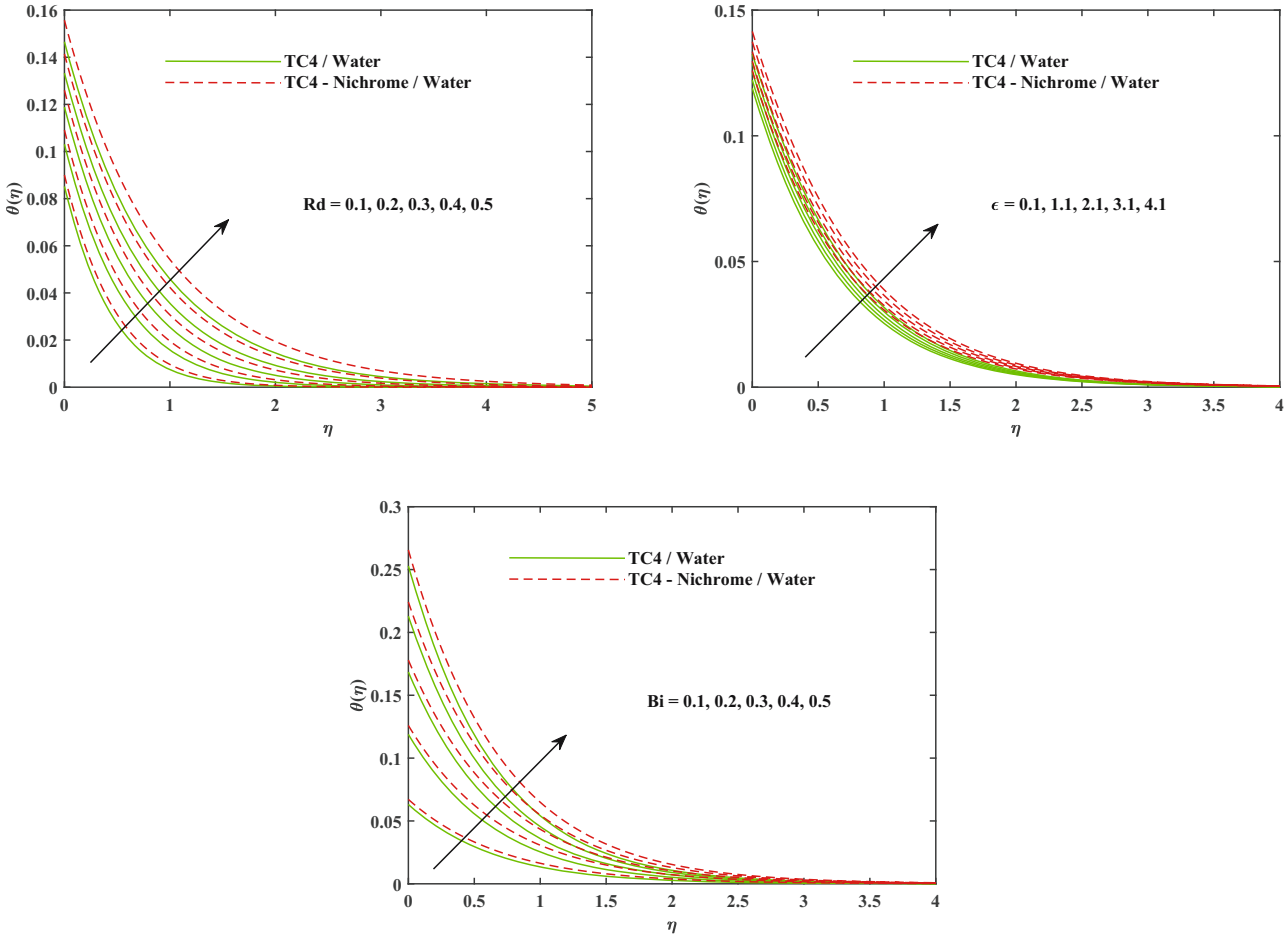

Figure 6: Temperature $\theta(\eta)$ fluctuation with Rd, ε, and Bi.

boundary-layer depth reduces. Moreover, the fluid's velocity is delayed as a response to the Williamson parameter. This is owing to the belief that the Williamson factor is the combination of relaxation and deceleration time.

Figure 3 displays the effects of varying the suction factor S and velocity slip factor β on the flow velocity $f'(\eta)$. The velocity $f'(\eta)$ diminishes as the suction parameter value increases. The velocity slip factor β exhibits a declining pattern in the velocity distribution; this could be due to an increment in slip impact that retards the liquid motion that depresses the fluid.

Figure 4 portrays the impact of nanoparticle concentration ϕ_2 on liquid velocity $f'(\eta)$ and temperature $\theta(\eta)$ when $\phi_1 = 0.0$ for TC4 and $\phi_1 = 0.01$ for TC4 + Nichrome. By boosting the valuation of ϕ_2, the velocity is reduced, so is the energy of the boundary-layer depth. Larger nanoparticles thickened the fluid, enabling the momentum boundary-layer to collapse. The amount of nanoparticles enhances the heat conductivity of nanoparticles. As a consequence of the rise in heat capacity, the energy boundary-layer revealed a decreasing tendency. Higher heat conductance of nanofluids, on the other hand, has a beneficial impact on fluid temperature since it improves with higher nanoparticle concentration.

In Figure 5, the heat variation of nanoparticles increases with an increase in the intensity of factor M, causing the heat boundary-layer to expand. This is also revealed that the variable M is inversely associated with the thickness of the nanofluid, and thus, boosting M diminishes velocity when the temperature of the liquid surges. As the Williamson factor λ increases, the heat boundary-layer extends, allowing the temperature to elevate leading to a rise in the elasticity stress factor.

Figure 6 explores the effects of the heat radiation factor Rd on the temperature dispersion $\theta(\eta)$ of Williamson nanofluids, indicating that the heat of the nanofluid improves with larger values of Rd = 0.1, 0.2, 0.3, 0.4, and 0.5. The depth of the heat boundary-layer improves as the temperature increases. Similarly, as ε values rise, the temperature dispersion rises. The temperature of the nanoparticles is also shown to expand as the Biot number increases. The smaller the Biot number, the greater the conductivity inside the surface, so the higher the Biot number, the greater the extreme conductivity at the exterior level. Because of the enhanced heat energy in nanoparticles, the temperature keeps rising. A rise in Bi promotes more heat transmission from the barrier to the liquid, thus increasing the conductivity of the boundary-layer.

Table 3 portrays that as the values of magnetic parameter M and suction factor S enhance, the skin friction factor $-f''(0)$ boosts for both TC4 nanofluid and TC4 + Nichrome nanofluids, whereas it declines for upsurging values of the Williamson parameter λ and velocity slip parameter β. In Table 4, the Nusselt number $-\theta'(0)$ increases for increasing values of Rd and Bi in both TC4 nanofluid and TC4 + Nichrome nanofluid cases; however, the Nusselt number $-\theta'(0)$ diminishes for upsurging values of ε.

Table 3: Results for skin friction factor $-f''(0)$

M	λ	S	β	TC4	TC4 + Nichrome
0.2	0.1	0.1	0.3	0.8038	0.8561
0.4				0.8659	0.9103
0.6				0.9198	0.9582
0.6	0.1			0.9198	0.9582
	0.3			0.8701	0.9027
	0.5			0.8118	0.8372
	0.1	0.1		0.9198	0.9582
		0.3		0.9668	1.0155
		0.5		1.0151	1.0742
		0.1	0.1	1.1828	1.2520
			0.3	0.9198	0.9582
			0.5	0.7951	0.7838

Table 4: Results for Nusselt number $-\theta'(0)$

Rd	ε	Bi	TC4	TC4 + Nichrome
0.1	0.1	0.2	0.2196	0.2051
0.3			0.2500	0.2328
0.5			0.2794	0.2595
0.3	0.1		0.2500	0.2328
	3.1		0.2471	0.2298
	6.1		0.2440	0.2264
	0.1	0.1	0.1329	0.1243
		0.2	0.2500	0.2328
		0.3	0.3539	0.3285

5 Conclusion

The two-dimensional MHD movement of the Williamson nanofluid was scrutinized with the influence of heat capacity varying from heat to heat radiation over the flexible surface. The complex equations that control velocity and heat, known as non-linear partial differential equations, are simplified into simpler equations called ordinary differential equations. This simplification is achieved by using a suitable transformation method called similarity transformation. The RK-4 approach was used to generate the computational model solution. The significance of the non-dimensional speed and heat gradient implications of the numerous physical factors under discussion is

depicted graphically. For every value of the individual governing factors, the coefficient of skin friction as well as the Nusselt number is presented in a tabulated form. Following a comprehensive analysis, we came to the preceding conclusion:

- An elevation in the Williamson factor, suction parameter, and nanoparticle concentration leads to a reduction in the velocity distribution.
- Nanoparticles are mostly engaged in fluids to enhance thermal characteristics. As an outcome, rising the density of nanoparticles boosts the temperature of the nanoparticles and thus the depth of the heat boundary-layer.
- TC4-Nichrome-water-based nanofluid is considered to be a better heat conductor than TC4-water-based nanofluid.
- Boosting the magnetic factor declines the depth of the velocity boundary-layer while improving the temperature distribution.
- An upsurge in the Williamson, thermal radiation factors, Biot number, and ε leads to an elevation in the temperature gradient.
- Skin friction improves with rising magnetic and suction factors for both TC4 and TC4-Nichrome nanofluids, but decreases with higher Williamson and velocity slip parameters.
- Heat transfer efficiency dropped as the quantity of the parameter ε expanded, but it expanded with the radiation parameter and Biot number boosted in both instances.

Acknowledgments: This research was supported by Research Supporting Project number (RSP2023R167), King Saud University, Riyadh, Saudi Arabia.

Funding information: This project was funded by King Saud University, Riyadh, Saudi Arabia.

Author contributions: All authors have accepted responsibility for the entire content of this manuscript and approved its submission.

Conflict of interest: The authors state no conflict of interest.

References

[1] Hazarika S, Ahmed S, Chamkha AJ. Investigation of nanoparticles Cu, Ag and Fe3O4 on thermophoresis and viscous dissipation of MHD nanofluid over a stretching sheet in a porous regime: a numerical modeling. Math Comput Simulat. 2021;182:819–37.

[2] Berrehal H, Sowmya G, Makinde OD. Shape effect of nanoparticles on MHD nanofluid flow over a stretching sheet in the presence of heat source/sink with entropy generation. Int J Numer Meth Heat Fluid Flow. 2022;32(5):1643–63.

[3] Tlili I, Samrat S, Sandeep N, Nabwey HA. Effect of nanoparticle shape on unsteady liquid film flow of MHD Oldroyd-B ferrofluid. Ain Shams Eng J. 2021;12(1):935–41.

[4] Zahmatkesh I, Sheremet M, Yang L, Heris SZ, Sharifpur M, Meyer JP, et al. Effect of nanoparticle shape on the performance of thermal systems utilizing nanofluids: a critical review. J Mol Liq. 2021;321:114430.

[5] Acharya N, Mabood F, Shahzad S, Badruddin I. Hydrothermal variations of radiative nanofluid flow by the influence of nanoparticles diameter and nanolayer. Int Commun Heat Mass Transf. 2022;130:105781.

[6] Abbas Z, Khaliq S. Calendering analysis of non-isothermal viscous nanofluid containing Cu-water nanoparticles using two counter-rotating rolls. J Plastic Film Sheeting. 2021;37(2):182–204.

[7] He JH, Abd Elazem NY. The carbon nanotube-embedded boundary-layer theory for energy harvesting. Facta Univ. Ser. Mech. Eng. 2022;20(2):211–35.

[8] Gorji N, Tanner B, Vijayaraghavan R, Danilewsky A, McNally P. Nondestructive in situ mapping of die surface displacements in encapsulated IC chip packages using x-ray diffraction imaging techniques. in: 2017 IEEE 67th Electronic Components and Technology Conference (ECTC). IEEE; 2017. p. 520–5.

[9] Williamson RV. The flow of pseudoplastic materials. Industr Eng Chemistry. 1929;21(11):1108–11.

[10] Yahya AU, Salamat N, Huang WH, Siddique I, Abdal S, Hussain S. Thermal characteristics for the flow of Williamson hybrid nanofluid (MoS2 + ZnO) based with engine oil over a stretched sheet. Case Stud Thermal Eng. 2021;26:101196.

[11] Abdelmalek Z, Khan SU, Waqas H, Riaz A, Khan IA, Tlili I. A mathematical model for bioconvection flow of Williamson nanofluid over a stretching cylinder featuring variable thermal conductivity, activation energy and second-order slip. J Thermal Anal Calorimetry. 2021;144(1):205–17.

[12] Wang F, Asjad MI, Ur Rehman S, Ali B, Hussain S, Gia TN, et al. MHD Williamson nanofluid flow over a slender elastic sheet of irregular thickness in the presence of bioconvection. Nanomaterials. 2021;11(9):2297.

[13] Li YX, Alshbool MH, Lv YP, Khan I, Khan MR, Issakhov A. Heat and mass transfer in MHD Williamson nanofluid flow over an exponentially porous stretching surface. Case Stud Thermal Eng. 2021;26:100975.

[14] Zhou SS, Khan MI, Qayyum S, Prasannakumara B, Kumar RN, Khan SU, et al. Nonlinear mixed convective Williamson nanofluid flow with the suspension of gyrotactic microorganisms. Int J Modern Phys B. 2021;35(12):2150145.

[15] Zubair T, Usman M, Hamid M, Sohail M, Nazir U, Nisar KS, et al. Computational analysis of radiative Williamson hybrid nanofluid comprising variable thermal conductivity. Japanese J Appl Phys. 2021;60(8):087004.

[16] Nazir U, Sadiq MA, Nawaz M. Non-Fourier thermal and mass transport in hybridnanoWilliamson fluid under chemical reaction in Forchheimer porous medium. Int Commun Heat Mass Transfer. 2021;127:105536.

[17] Eshgarf H, Kalbasi R, Maleki A, Shadloo MS, Karimipour A. A review on the properties, preparation, models and stability

of hybrid nanofluids to optimize energy consumption. J Thermal Anal Calorimetry. 2021;144(5):1959–83.
[18] Sathyamurthy R, Kabeel A, Chamkha A, Karthick A, Manokar AM, Sumithra M. Experimental investigation on cooling the photovoltaic panel using hybrid nanofluids. Appl Nanosci. 2021;11(2):363–74.
[19] Abid M, Khan MS, Ratlamwala TAH, Malik MN, Ali HM, Cheok Q. Thermodynamic analysis and comparison of different absorption cycles driven by evacuated tube solar collector utilizing hybrid nanofluids. Energy Conversion Management. 2021;246:114673.
[20] Alfvén H. Existence of electromagnetic-hydrodynamic waves. Nature. 1942;150(3805):405–6.
[21] Alblawi A, Keyani S, Nadeem S, Issakhov A, Alarifi IM. Ciliary flow of casson nanofluid with the influence of MHD having carbon nanotubes. Current Nanosci. 2021;17(3):447–62.
[22] Sabu AS, Areekara S, Mathew A. Effects of multislip and distinct heat source on MHD Carreau nanofluid flow past an elongating cylinder using the statistical method. Heat Transfer. 2021;50(6):5652–73.
[23] Rasheed HU, Islam S, Helmi MM, Alsallami S, Khan Z, Khan I. An analytical study of internal heating and chemical reaction effects on MHD flow of nanofluid with convective conditions. Crystals. 2021;11(12):1523.
[24] Makkar V, Batra P. Numerical simulation of MHD convective nanofluid flow with buoyancy forces over three dimensional exponential stretching surface. Materials Today: Proceedings. 2022;52(3):810–7.
[25] Jimoh MO. Reacting magnetohydrodynamic (MHD) flow of nanofluids with variable thermal conductivity and viscosity in presence of thermal radiation. Nigeria: Kwara State University; 2021.
[26] Ali A, Kanwal T, Awais M, Shah Z, Kumam P, Thounthong P. Impact of thermal radiation and non-uniform heat flux on MHD hybrid nanofluid along a stretching cylinder. Scientific Reports. 2021;11(1):1–14.
[27] Nawaz Khan M, Ahmad I, Ahmad H. A radial basis function collocation method for space-dependent inverse heat problems. J Appl Comput Mech. 2020;6(Spec. issue):1187–99.
[28] Ahmad H, Khan TA, Yao SW. An efficient approach for the numerical solution of fifth-order KdV equations. Open Math. 2020;18(1):738–48.
[29] Ahmad H, Khan TA. Variational iteration algorithm I with an auxiliary parameter for the solution of differential equations of motion for simple and damped mass-spring systems. Noise Vibrat Worldwide. 2020;51(1–2):12–20.
[30] Akgü l A, Ahmad H. Reproducing kernel method for Fangzhuas oscillator for water collection from air. Math Meth Appl Sci. 2020. doi: 10.1002/mma.6853.
[31] Liu X, Ahsan M, Ahmad M, Nisar M, Liu X, Ahmad I, et al. Applications of Haar wavelet-finite difference hybrid method and its convergence for hyperbolic non-linear Schrödinger equation with energy and mass conversion. Energies. 2021;14(23):7831.
[32] Wang F, Zhang J, Ahmad I, Farooq A, Ahmad H. A novel meshfree strategy for a viscous wave equation with variable coefficients. Frontiers Phys. 2021;9:701512.
[33] Ahmad I, Seadawy AR, Ahmad H, Thounthong P, Wang F. Numerical study of multi-dimensional hyperbolic telegraph equations arising in nuclear material science via an efficient local meshless method. Int J Nonlinear Sci Numer Simulat. 2022;23(1):115–22.
[34] Shakeel M, Khan MN, Ahmad I, Ahmad H, Jarasthitikulchai N, Sudsutad W. Local meshless collocation scheme for numerical simulation of space fractional PDE. Thermal Sci. 2023;27(Spec. issue 1):101–9.
[35] Ahsan M, Khan AA, Dinibutun S, Ahmad I, Ahmad H, Jarasthitikulchai N, et al. The Haar wavelets based numerical solution of Reccati equation with integral boundary condition. Thermal Sci. 2023;27(Spec. issue 1):93–100.
[36] Irshad H, Shakeel M, Ahmad I, Ahmad H, Tearnbucha C, Sudsutad W.. Simulation of generalized time fractional Gardner equation utilizing in plasma physics for non-linear propagation of ion-acoustic waves. Thermal Sci. 2023;27(Spec. issue 1):121–8.
[37] Almutairi B, Ahmad I, Almohsen B, Ahmad H, Ozsahin DU. Numerical simulations of time-fractional PDEs arising in mathematics and physics using the local Meshless differential quadrature method. Thermal Sci. 2023;27(Spec. issue 1):263–72.
[38] Prasad K, Rajashekhar C, Mebarek-Oudina F, Animasaun I, Makinde O, Vajravelu K, et al. Unsteady magnetohydrodynamic convective flow of a nanoliquid via a radially stretched riga area via optimal homotopy analysis method. J Nanofluids. 2022;11(1):84–98.
[39] Farooq M, Ahmad Z, Ahmad H, Zeb M, Aouaini F, Ayaz M. Homotopy analysis methods with applications to thin-film flow of a magnetohydrodynamic-modified second grade fluid. Modern Phys Lett B. 2022;36(19):2150617.
[40] Wang F, Ali SN, Ahmad I, Ahmad H, Alam KM, Thounthong P. Solution of Burgers equation appears in fluid mechanics by multistage optimal homotopy asymptotic method. Thermal Sci. 2022;26(1 Part B):815–21.
[41] Ali SN, Ahmad I, Abu-Zinadah H, Mohamed KK, Ahmad H. Multistage optimal homotopy asymptotic method for the K(2, 2) equation arising in solitary waves theory. Thermal Sci. 2021;25(Spec. issue 2):199–205.
[42] Khan Y, Abdal S, Hussain S, Siddique I. Numerical simulation for thermal enhancement of H2O + Ethyl Glycol base hybrid nanofluid comprising GO.(Ag, AA7072, MoS2) nano entities due to a stretched sheet. AIMS Math. 2023;8(5):11221–37.
[43] Abdal S, Chukwu C. Significance of variable viscosity for time-dependent flow of hybrid nanofluids due to spinning surface. Alexandr Eng J. 2023;71:551–63.